J. Appl. Comput. Mech., 8(4) (2022) 1208-1221
DOI: 10.22055/JACM.2021.38390.3215

ISSN: 2383-4536
jacm.scu.ac.ir

Shahid Chamran
University of Ahvaz

Journal of
Applied and Computational Mechanics

Research Paper

Magneto Casson-Carreau Fluid Flow through a Circular Porous Cylinder with Partial Slip

N. Nagendra[1], B. Venkateswarlu[2], Z. Boulahia[3], CH. Amanulla[4], G.K. Ramesh[5]

[1] Department of Mathematics, Sri Sai Institute of Technology and Science, Rayachoty, A.P., 516270, India, Email: nagsvu76@gmail.com

[2] Department of Mathematics, Walchand Institute of Technology, Solapur, M.H., 413006, India, Email: bvenkateswarlu.maths@gmail.com

[3] Laboratory of Mechanics, Faculty of Sciences, Hassan II University, BP, Maarif Casablanca, 5366, Morocco, Email: Boulahia.zoubair@gmail.com

[4] Department of Mathematics, Sreenivasa Institute of Technology and Management Studies, Chittoor, A.P., 517125, India, Email: amanullamsc@gmail.com

[5] Department of Mathematics, K.L.E Society's J.T. College, Gadag, Karnataka, 582101, India, Email: gkrmaths@gmail.com

Received August 28 2021; Revised November 06 2021; Accepted for publication November 08 2021.
Corresponding author: B. Venkateswarlu (bvenkateswarlu.maths@gmail.com)

Abstract. In the current study, a comparative analysis of two-dimensional heat transfer by the free convective flow of non-Newtonian Casson and Carreau fluid in electro-conductive polymer on the outside surface of a horizontal circular cylinder under slip and radial magnetic field effects is regarded. The Casson and Carreau fluid model formulation were first developed for the problem of the boundary layer of the horizontal circular cylinder and by using non-similarity transformations, the combined governing partial differential equations are translated into ordinary differential equations. The differential equations obtained are resolved by the Keller Box Method (KBM). The impact of the key parameters, the rate of heat transfer and skin friction is evaluated through graphs and tables. The result reveals that an increase in magnetic number decreases the velocity field of both Casson and Carreau fluid also Casson fluid is higher values when compared to Carreau fluid in variation of magnetic number.

Keywords: MHD, Casson-Carreau fluid, Circular cylinder, Porous medium, Keller-Box method.

1. Introduction

The non-Newtonian fluids are famous due to diverse classical properties. With complicated nature and distinct rheology, the interest of scientists is to explore more interesting features of such materials. The nature of non-Newtonian liquids are noticed to be entirely distinct as compared to the viscous liquids. The non-Newtonian liquids play one of the major contributions in various manufacturing industries, chemical processing and engineering. The real valuable examples associated with the non-Newtonian materials are observed like starch suspension, cosmetics, molten, medicine, paints, blood, etc. The characterization of such materials is usually presented in three types like rate type, integral and differential fluid types. Numerous advanced designing applications include the investigation of non-Newtonian liquids. This includes mud drilling for petroleum [1], biological gels [2], polymer [3] and food [4] processing. Also, the heat transfer flow of non-Newtonian fluid is of extraordinary impact in hot rolling, glass sheets blowing and paper production [5-7]. While basic, the Casson model is useful in simulating a variety of polymers, such as alcohol, flood polymers used in enhanced oil recovery [8]. Tassaddiq et al. [9] presented an application of Newtonian heating for Casson fluid flow by using a fractional operator. Ramzan et al. [10] explored the MHD Casson nanofluid flow in an elastic cylinder due to Newtonian heating. They found that the higher hotness happened with the case of Newtonian heating. The rheological properties of non-Newtonian liquids can be observed as no particular constitutive association among stress and pace of strain. Hence, there are quite a few non-Newtonian fluid models, but Casson liquid are the most straightforward model for rheological impacts of viscoelastic fluids. Nazeer et al. [11-12] imposed the analytical and numerical schemes for the convective flow of non-Newtonian Eyring-Powell fluid in a porous canal. Ansari et al. [13] and Trivedi et al. [14] imposed the Quasilinearization scheme for the convective flow of Casson nanofluid and they originate that the speed and warmth display an opposite behaviour with Casson parameter. Temperature dependent viscosity of hybrid nanofluid due to porous plate/sheet was investigated by Venkateswarlu and Satya Narayana [15-16]. Their work performs biomedical and engineering applications like: drugs delivery, cancer therapy and cooling/heating process, etc.

The Casson liquid model was initially acquainted with portraying printing inks by Casson [17]. It is a viscoelastic liquid model which shows shear diminishing attributes, yield worry (beneath which no stream happens) and high shear thickness as expounded by Bird et al. [18]. This model keeps an eye on a Newtonian liquid at a high divider shear push, i.e. at the point when the divider stretch is far more noteworthy than yield push. To enhance and preparing of many sorts of polymers, various examiners have directed recreations of Casson stream flow utilizing numerous computational and diagnostic strategies. These

Published online: November 16 2021

examinations have included warmth exchange (essential for warm treatment), mass exchange (basic to doping change of polymers), gooey warming, magnetohydrodynamics (for electro-conductive polymers) and numerous other marvels. Hayat et al. [19] examined the dissipative heat transfer characteristics of a Casson fluid through an elastic sheet by using homotopy analysis. Nasir et al. [20] analyzed the heat and mass and transfer between long parallel and vertical wavy walls under convective boundary conditions in the transient flow of Casson fluid. Venkateswarlu and Satya Narayana [21-22] carried out the shooting scheme for heat and mass transfer flow of Casson nanofluid and found that heat and mass transfer rates are controlled by the thermal conductivity parameter.

With rising shear stretch speeds, the thickness of Carreau fluids is reduced and this model has discovered some renown in building reenactments. The movers of Carreau fluid and the diffusion of heat between two concentric cylinders were studied by Khellaf and Lauriat [23]. The MHD non-Newtonian Carreau fluid flow over a convective surface was studied by Khan et al. [24]. In Falkner-Skan Carreau liquid stream, the momentum and heat transfer through an isothermal wedge was investigated by Raju and Sandeep [25]. Theoretically, Akbar et al. [26] are researching MHD stagnation-point movement of Carreau fluid over a shrinking layer. Abbas et al. [27] have studied a Carreau fluid flow by homotopy analysis method. Azam et al. [28] and Song & Co [29] scrutinized the melting heat transfer of bioconvection nanofluid flow by carrying activation energy with thermo diffusion and Brownian motion. Malik et al. [30] presented heat transfer flow of Williamson fluid caused by cylinder spreading in the midst of a homogeneous-heterogeneous reaction. Activation energy analysis in an axisymmetric flow of Williamson nanofluid was presented by Azam et al. [31-32]. It is devoted that the nanoparticle volume fraction is rising by the cause of activation energy. Rehman et al. [33] explored dual convection of Williamson fluid with chemical reactions along an angled stretching cylinder. By considering multiple flow geometries and varying physical results [34-39] [34-38] studied the properties of non-Newtonian Carreau fluids. Santoshi et al. [40], Nagendra et al. [41] and Amanulla et al. [42] examined the non-Newtonian Casson-Carreau nanofluid by adapting convective conditions. The slip parameter plays vital role in the heat transfer rate, friction factor and velocity for both the fluid cases. Liu and Gehde [43] considered wall slip in thermal polymer manufacturing. The finite element formula and closed type solutions for the effect of wall slip in tapered dies on Power-law fluids along with pressure drop were proposed by Hatzikiriakos and Mitsoulis [44]. The first important study of laminar slip-flow thermal transfer for uniform heat flux pipes was reported by Sparrow et al. [45]. They noted that the momentum slip works to boost the flow of heat while reducing Shift of heat by thermal slip. Subba Rao et al. [46] exposed the slip effects of Casson fluids with buoyancy property on thermal convection boundary layer flow. Uddin et al. [47] used Maple software to conduct several slip effects on bio-convection flows of 3D nanofluids. Recently, many authors [48-50] studied the Casson-Carreau fluid flows in various geometrical approaches.

The flow over a plane or parabolic or any other regions was the subject of all the above studies. In this work, we research the two-dimensional magneto-hydrodynamic Casson and Carreau fluid flowing past a circular cylinder under the slip effects. Graphically, the influence of various quantities of the thermal fields, flow of fluids, the skin friction and rate of heat transfer are seen. Tabular findings for wall friction and Nusselt number are recorded for.

2. Formulation and Physical Model

The magneto-hydrodynamic (MHD) steady free heat transfer flow of convection from the horizontal circular cylinder of Casson and Carreau fluid is studied. The flow model and related co-ordinate system are seen in Figure 1. Incompressible and a homogenous dilute solution is taken to be the nanofluid fluid. B_0 is the magnetic field of strength and usually applied to the flow. From the lowest point, the x-coordinate is determined via the diameter of horizontal cylinder and the y-coordinate is determined normal to the surface, with 'a' that denotes a horizontal cylinder radius. With respect to the vertical $0 \le \Phi \le \pi$ and $\Phi = x/a$ is the y-axis orientation angle. The g acts downward with gravitational acceleration. The fluid and horizontal cylinder are both held in the similar heat initially. They are instantaneously elevated to warmth $T_w > T_\infty$ that is the fluid's ambient warmth that stays unchanged.

The stress tensor of Carreau fluid is defined as

$$\bar{\tau}_{ij} = \eta_0 \left(1 + \frac{(n-1)}{2}(\Gamma\bar{\dot{\gamma}})^2 \bar{\dot{\gamma}}_{ij}\right), \tag{1}$$

where $\bar{\tau}_{ij}$ is the additional stress tensor, η_0 is the viscosity of the zero shear rate, Γ is the time value, n is the power-law index and $\bar{\dot{\gamma}}$ is described as

$$\bar{\dot{\gamma}} = \sqrt{\frac{1}{2}\sum_i \sum_j \overline{\dot{\gamma}_{ij}\dot{\gamma}_{ij}}} = \sqrt{\frac{1}{2}\Pi}, \tag{2}$$

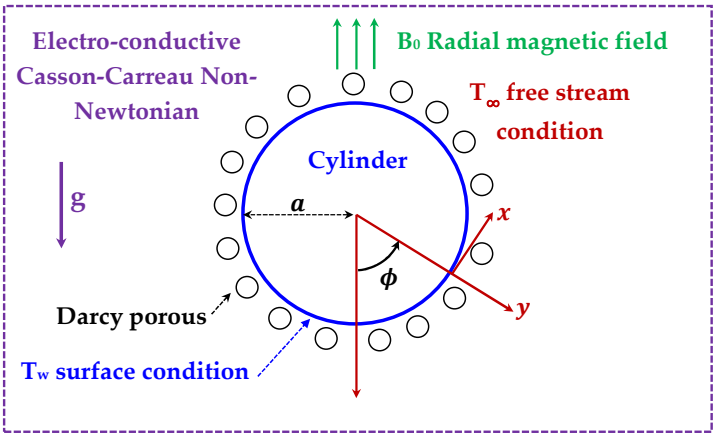

Fig. 1. Physical model circular cylinder

Casson fluids have two-dimensional steady flows offered by (see Refs. [51-55])

$$\tau_{ij}=\begin{cases}2\left(\mu_B+\dfrac{p_y}{\sqrt{2\pi}}\right)e_{ij}, & \pi\geq\pi_c\\ 2\left(\mu_B+\dfrac{p_y}{\sqrt{2\pi_c}}\right)e_{ij}, & \pi<\pi_c\end{cases}, \tag{3}$$

where $\prod$ is the second invariant strain tensor. Based on the above suppositions, the governing equations for continuity, momentum and energy (see Refs. [41-42]) are defined as

$$\frac{\partial u}{\partial x}+\frac{\partial v}{\partial y}=0, \tag{4}$$

$$u\frac{\partial u}{\partial x}+v\frac{\partial u}{\partial y}=\nu\left\{\left(1+\frac{1}{\beta}\right)\frac{\partial^2 u}{\partial y^2}+\frac{3}{2}(n-1)\Gamma^2\left(\frac{\partial u}{\partial y}\right)^2\frac{\partial^2 u}{\partial y^2}\right\}+g\beta^*(T-T_\infty)\sin\left(\frac{x}{a}\right)-\frac{\sigma B_0^2}{\rho}u-\frac{\nu}{K}u-\Gamma u^2, \tag{5}$$

$$u\frac{\partial T}{\partial x}+v\frac{\partial T}{\partial y}=\alpha\frac{\partial^2 T}{\partial y^2}, \tag{6}$$

At the cylinder surface and in the free stream, the boundary conditions placed are

$$\begin{aligned}&\text{at}\quad y=0,\quad u=N_0\frac{\partial u}{\partial y},\quad v=0,\quad T=T_w+K_0\frac{\partial T}{\partial y},\\ &\text{as}\quad y\to\infty,\quad u\to 0,\ v\to 0,\ T\to T_\infty,\end{aligned} \tag{7}$$

Here N_0 is the speed slip factor, K_0 is the thermal slip factor and T_∞ is the temperature of the free stream. One can retrieve the no-slip case for $N_0=0=K_0$.

The Cauchy-Riemann equations $u=\partial\psi/\partial y$ and $v=-\partial\psi/\partial x$ define the stream function ψ and the continuity equation is therefore immediately fulfilled.

Appropriate non-dimensional quantities are defined as

$$\eta=\frac{y}{a}Gr^{1/4},\quad \xi=\frac{x}{a}\quad f(\xi,\eta)=\frac{\psi}{\nu\xi Gr^{1/4}},\quad \theta(\xi,\eta)=\frac{T-T_\infty}{T_w-T_\infty}, \tag{8}$$

The transformed equations for energy and concentration in the boundary layer appear as

$$\left(1+\frac{1}{\beta}\right)f'''+\frac{3}{2}(n-1)We f''^2 f'''-(1+\Lambda\xi)f'^2+\frac{\sin\xi}{\xi}\theta-\left(M+\frac{1}{Da}\right)f'=\xi\left(f'\frac{\partial f'}{\partial\xi}-f''\frac{\partial f}{\partial\xi}\right), \tag{9}$$

$$\frac{\theta''}{Pr}+f\theta'=\xi\left(f'\frac{\partial\theta}{\partial\xi}-\theta'\frac{\partial f}{\partial\xi}\right), \tag{10}$$

The related dimensionless boundary conditions that have been transformed are

$$\begin{aligned}&f=0,\ f'=f''(0)\left(1+\frac{1}{\beta}\right)S_f,\ \theta=1+\theta'(0)S_T,\quad \text{at}\quad \eta=0\\ &f'\to 0,\quad \theta\to 0,\quad \text{as}\ \eta\to\infty\end{aligned} \tag{11}$$

and the skin friction and Nusselt number is reduce to

$$Gr^{-3/4}C_f=\xi f''(\xi,0)\left(\left(1+\frac{1}{\beta}\right)+\frac{3}{2}(n-1)We f''^2(\xi,0)\right), \tag{12}$$

$$Gr^{-1/4}Nu=-\theta'(\xi,0), \tag{13}$$

3. Keller-Box Implicit Method

In a coordinate system, the coupled boundary layer equations remain highly nonlinear. Therefore, to solve the boundary value problem described by Eqs. (9)-(10) with boundary conditions (11), a numerical procedure the Keller-Box implicit difference scheme is implemented. In Cebeci and Bradshaw [56] and Keller [57], this approach was defined succinctly. However, very few of these articles have presented researchers with advice on customizing the Keller-box scheme for heat transfer problems. We also included descriptions of the method of discretization below. The following four steps include the application of the Keller scheme

Decrease to N first order equations of the N^{th} order PDE system

(a) Discretization of Finite Difference
(b) Algebraic equations of Non-Linear Keller Quasilinearization
(c) Elimination of LKAE by BT

Taking into account the subsequent alteration of variables

$$\frac{\partial f}{\partial \eta} = u = f', \qquad \frac{\partial u}{\partial \eta} = v = u', \qquad \frac{\partial \theta}{\partial \eta} = t = \theta', \tag{14}$$

Eqs. (9) and (10) can be concentrated to the subsequent structure as

$$\left(1+\frac{1}{\beta}\right)v' + fv + \frac{3}{2}(n-1)We\,vv' - u^2 + \frac{1}{\xi}\sin(\xi)s - Mu = \left(\frac{\partial u}{\partial \xi}u - \frac{\partial f}{\partial \xi}v\right)\xi, \tag{15}$$

$$Pr^{-1}t' + ft = \xi\left(u\frac{\partial s}{\partial \xi} - t\frac{\partial f}{\partial \xi}\right), \tag{16}$$

Here, the primes imply distinction in relation to η and $\theta = s$. The boundary conditions (15) becoming, in terms of the dependent variables

$$\begin{aligned} &f = 0, && f' = S_f f''(0), && \theta = 1 + \theta'(0)S_T, && \text{at } \eta = 0 \\ &&& f' \to 0, && \theta \to 0, && \text{as } \eta \to \infty \end{aligned}, \tag{17}$$

As seen in Fig. 2, a 2-D computational mesh is imposed on the plane of $\xi - \eta$. The method of stepping is described by

$$\eta_j = \eta_{j-1} + h_j, \qquad 1 \le j \le J \quad \eta_j \equiv \eta_\infty, \qquad \eta_0 = 0, \tag{18}$$

$$\xi^n = \xi^{n-1} + k_n, \qquad 1 \le n \le N, \qquad \xi^0 = 0, \tag{19}$$

Here, k_n is the step distance in the ξ direction and h_j is the step distances in the η direction. If g_j^n denotes the value of any variable at (η_j, ξ^n), then the variable and derivative terms appeared in Eqs. (17) and (18) at $(\eta_{j-1/2}, \xi^{n-1/2})$ are replaced by

$$\left.\begin{aligned} g_{j-1/2}^{n-1/2} &= \frac{1}{4}\left(g_j^n + g_{j-1}^n + g_j^{n-1} + g_{j-1}^{n-1}\right) \\ \left(\frac{\partial g}{\partial \eta}\right)_{j-1/2}^{n-1/2} &= \frac{1}{2h_j}\left(g_j^n - g_{j-1}^n + g_j^{n-1} - g_{j-1}^{n-1}\right) \\ \left(\frac{\partial g}{\partial \xi}\right)_{j-1/2}^{n-1/2} &= \frac{1}{2k^n}\left(g_j^n - g_{j-1}^n + g_j^{n-1} - g_{j-1}^{n-1}\right) \end{aligned}\right\}, \tag{20}$$

At the mid-point $(\eta_{j-1/2}, \xi^n)$, the finite difference approximations for the variables u, v, t are given as

$$t_{j-1/2}^n = h_j^{-1}\left(s_j^n - s_{j-1}^n\right), \qquad v_{j-1/2}^n = h_j^{-1}\left(u_j^n - u_{j-1}^n\right), \qquad u_{j-1/2}^n = h_j^{-1}\left(f_j^n - f_{j-1}^n\right), \tag{21}$$

Consequently, the suitable discretized structure of Eqs. (17) & (18) are written as follows

$$\left.\begin{aligned} &\left(1+\frac{1}{\beta}\right)\left(v_j - v_{j-1}\right) + (1+\alpha)\frac{h_j}{4}\left(f_j + f_{j-1}\right)\left(v_j + v_{j-1}\right) - \frac{(1+\alpha+\Lambda\xi)h_j}{4}\left(u_j + u_{j-1}\right)^2 + \frac{3(n-1)We}{4}\left[\left(v_j\right)^2 - \left(v_{j-1}\right)^2\right] \\ &+ \frac{Ah_j}{2}\left(s_j + s_{j-1}\right) - \frac{h_j}{2}\left(M + \frac{1}{Da}\right)\left(u_j + u_{j-1}\right) - \frac{\alpha h_j}{2}f_{j-1/2}^{n-1}\left(v_j + v_{j-1}\right) + \frac{\alpha h_j}{2}v_{j-1/2}^{n-1}\left(f_j + f_{j-1}\right) = [R_1]_{j-1/2}^{n-1} \end{aligned}\right\}, \tag{22}$$

$$\left.\begin{aligned} &Pr^{-1}\left(t_j - t_{j-1}\right) + (1+\alpha)\frac{h_j}{4}\left[\left(f_j + f_{j-1}\right)\left(t_j + t_{j-1}\right)\right] - \frac{\alpha h_j}{4}\left[\left(u_j + u_{j-1}\right)\left(s_j + s_{j-1}\right)\right] + \frac{\alpha h_j}{2}s_{j-1/2}^{n-1}\left(u_j + u_{j-1}\right) \\ &- \frac{\alpha h_j}{2}u_{j-1/2}^{n-1}\left(s_j + s_{j-1}\right) - \frac{\alpha h_j}{2}f_{j-1/2}^{n-1}\left(t_j + t_{j-1}\right) + \frac{\alpha h_j}{2}t_{j-1/2}^{n-1}\left(f_j + f_{j-1}\right) = [R_2]_{j-1/2}^{n-1} \end{aligned}\right\}, \tag{23}$$

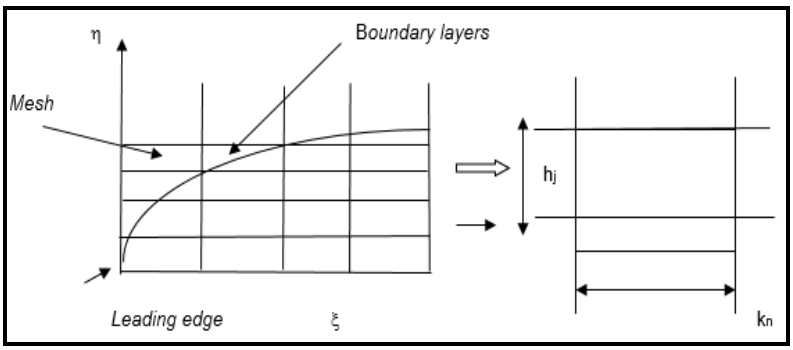

Fig. 2. Boundary layer mesh and Keller Box element

Here, the following abbreviations are used

$$\frac{-[R_1]_{j-1/2}^{n-1}}{h_j}=\left(1+\frac{1}{\beta}\right)\left(\frac{v_j-v_{j-1}}{h_j}\right)+(1-\alpha)\left(f_{j-1/2}\ v_{j-1/2}\right)+\frac{3(n-1)\ We}{2}\left(v_{j-1}\ v'_{j-1/2}\right)+(1-\alpha+\Lambda\xi)\left(u_{j-1/2}\right)^2+As_{j-1/2}-\left(M+\frac{1}{Da}\right)u_{j-1/2}\Bigg\}, \tag{24}$$

$$\alpha=\frac{\xi^{n-1/2}}{k_n}\ ,\ A=\frac{\sin\left(\xi^{n-1/2}\right)}{\xi^{n-1/2}}, \tag{25}$$

The system of Eqs. (28) and (29) are solved subject to the following boundary conditions

$$f_0^n=u_0^n=0,\quad \theta_0^n=1,\quad u_j^n=0,\quad v_j^n=0,\quad \theta_j^n=0\ , \tag{26}$$

By the way of Newton's method, the algebraic equations are linearized and then solved by the process of block elimination. The accuracy of computations is affected in both ways by different mesh points. A greater quantity of network points is chosen after playing with different grid sizes in the path, whereas slightly fewer mesh points are used in the path. The mathematical value of $\eta_{\max}$ has been set to 10, defining a suitably huge charge at which the border line situation is met, while the partial value of $\xi_{\max}$ is set to 3 for the domain of this stream. Consequently, meshes autonomy is obtained in the existing computations. Using the K-B & F-D scheme with the help of MATLAB tools, the present problem is solved.

Assuming that f_{j-1}^{n-1}, u_{j-1}^{n-1}, v_{j-1}^{n-1}, s_{j-1}^{n-1} and t_{j-1}^{n-1} are designed for $1\le j\le J$, the discretized Eqs. (25)-(29) make up a system of $5J+5$ equations, which is collected by the $5J+5$ unknowns f_{j-1}^{n-1}, u_{j-1}^{n-1}, v_{j-1}^{n-1}, s_{j-1}^{n-1} and t_{j-1}^{n-1}, where $0\le j\le J$. By means of Newton's method, the corresponding algebraic system is linearized and then resolved by using the K-B technique, which Cebeci and Bradshaw [56] have more specifically explained [57], Taking the initial relationship with a particular set of converged solutions at $\xi=\xi^n$. We first recommend a series of estimate for the functions f,u,v,s and t that are categorically convergent to start the process with $\xi=0$. Such profiles are then used with second-order precision in the Keller-Box scheme to determine the proper solution step by step along the state line coating. The iterative method is stopped for a given ξ to give the final velocity and temperature distributions when the difference in the calculation of these functions becomes less than 10^{-5} in the next procedure, i.e. $\left|\delta f^i\right|\le 10^{-5}$, where the number of iterations is denoted by the superscript i.

The convergence rate of Eqs. (25)-(29) solutions is quadratic for laminar flows, providing that the initial approximation of the optimal solution is relatively similar to the final solution. Four distinct spacing formulas demonstrate that the convergence rate of the solutions on behalf of initial profiles with standard iterations is quadratic in both situations. Due to fact that Newton's approach is used to linearize the nonlinear system and the convergence rate of the solutions should be quadratic with the right preliminary guess ξ^n normally obtained from a solution at ξ^{n-1}; it can be used to evaluate the code for potential programming errors and to assist in the choice of space $\Delta\xi$ on the downstream track.

The calculations were conducted in range $0\le\xi\le 0.4$ with consistent spacing $\Delta\xi$ corresponding to 0.01, 0.02, 0.04 and 0.08 to research the influence of space $\Delta\xi$ on the convergence rate solutions. The results obtained with $\Delta\xi=0.08$, at each ξ station, the convergent rate of the solutions was basically quadratic. A tread dimension starting 0.02 to 0.04 is appropriate to give reliable and equal findings in most laminar boundary layer flows. In reality, we can also go up to $\Delta\xi=0.1$ in the present problem and still get reliable and comparable outcomes. Merkin [58] has also effectively used this particular attribute of $\Delta\xi=0.1$.

In favor of laminar flow calculations, mainly in the laminar state line stratum, an identical network from corner to corner the boundary is fitting. However, the Keller-Box solution is special in which separate spaces in both ξ and η guidelines be able to use.

4. Outcome and Explanation

Throughout the analysis, these values are preserved as constant except for the different quantities like: magnetic field parameter (M), velocity and thermal slip parameters (S_f, S_T), Prandtl number (Pr), Darcian porosity (Da), Forchheimer inertial drag parameter (Λ) on the velocity and temperature fields along with the heat transfer rate (Nu) and skin friction coefficient (C_f) as mentioned in the figures and tables. The red and green lines represent the cases of $n=1$ and β over a cylinder in this analysis.

In order to check the exactness of the K-B solutions and calculations, earlier results stated by Merkin [58], Molla et al.[59] and Javed et al.[60] are compared with the coefficients of skin friction (C_f) and heat transfer (Nu) of Newtonian fluid (i.e. $We=0$), respectively, for different parameter ξ values in the case of $\Pr=1.0$, $S_f=S_T=M=0$. Table 1 summarizes the findings of this comparison. There is a very close correlation between the effects of the Keller-Box estimation and the solutions of Merkin [58], Molla et al. [59] and Javed et al. [60]. The K-B numerical code used in this analysis thus contributes to numerical findings that are very reliable.

Both the Casson and Carreau fluid cases, Fig. 3(a-b) indicate the influence of the magnetic field parameter (M) on the velocity and temperature fields. It is apparent that with growth M in the temperature fields are increased and velocity fields are decreased. An increase of M in the physical point of view produces a resistant form of opposing force in the direction of flow that causes the velocity boundary layer to decrease. The magnetic field, thus serves as a retarding force along with the slip effect and regulates the velocity of the fluid, which is useful in various applications such as electromagnetic cable insulation, MHD power generation and metal, etc.

Table 1. Comparison of skin friction and Nusselt number with those of Merkin[58], Molla et al. [59] and Javed et al. [60] while $\mathrm{Pr} = 1.0$ and $M = S_f = S_\tau = We = 0.0$

ξ	C_f				Nu			
	[58]	[59]	[60]	Present Solutions	[58]	[59]	[60]	Present Solutions
0	0.0000	0.0000	0.0000	0.0000	0.4214	0.4216	0.4215	0.4218
$\pi/6$	0.4151	0.4139	0.4150	0.4247	0.4161	0.4163	0.4163	0.4165
$\pi/3$	0.7558	0.7527	0.7557	0.7559	0.4007	0.4006	0.4009	0.4011
$\pi/2$	0.9579	0.9526	0.9578	0.9576	0.3745	0.3741	0.3747	0.3752
$2\pi/3$	0.9756	0.9677	0.9555	0.9551	0.3364	0.3355	0.3355	0.3354
$5\pi/6$	0.7822	0.7717	0.7822	0.7821	0.2825	0.2810	0.2824	0.2839
π	0.3391	0.3238	0.3388	0.3385	0.1945	0.1911	0.1943	0.1954

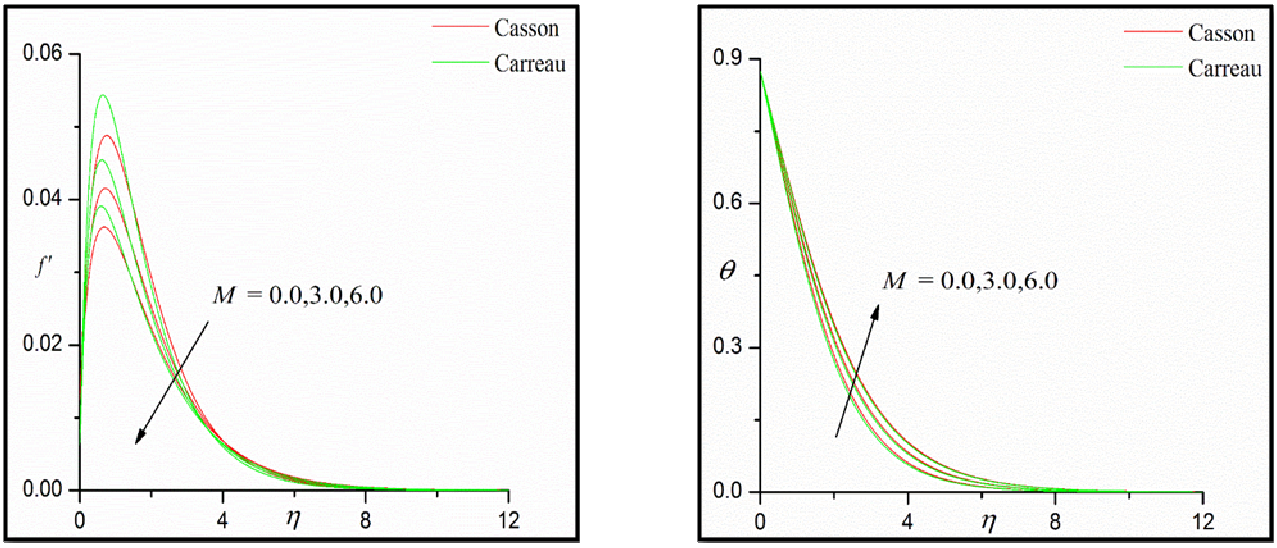

(a) (b)

Fig. 3. Effects of magnetic field parameter on the (a) velocity (b) temperature

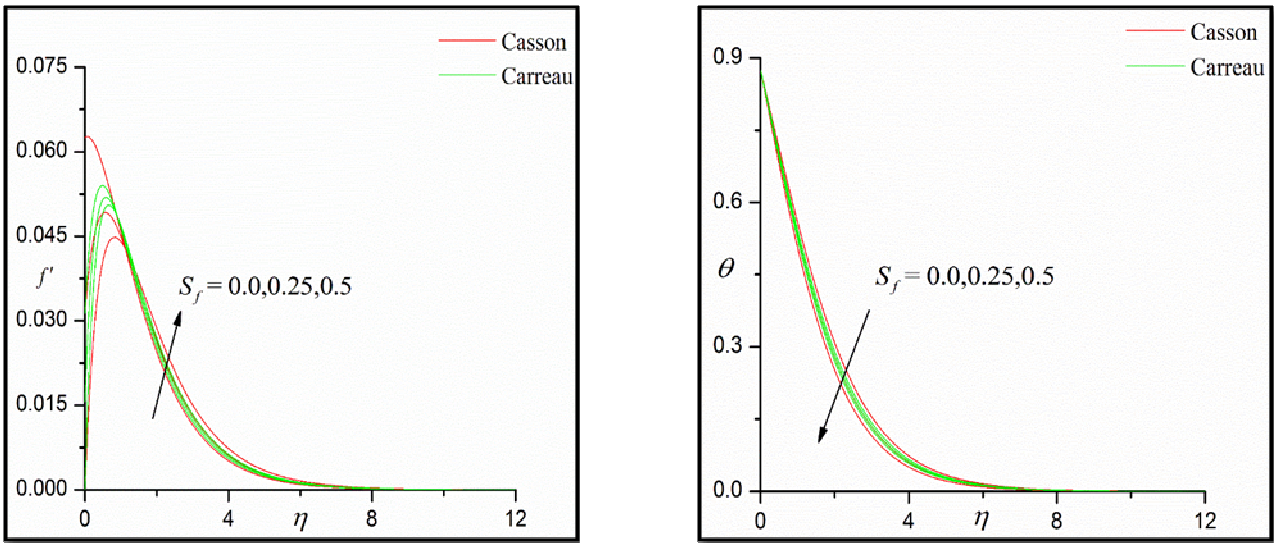

(a) (b)

Fig. 4. Effects of velocity slip parameter on the (a) velocity (b) temperature

In Fig. 4(a-b) for both the Carreau and Casson fluid cases, the variance in velocity and temperature fields due to the effect of velocity slip (S_f) is presented. A progress in S_f, the findings indicate a decrease in velocity and an increase in temperature fields, is noted. The flow velocity is then decreased by a slip parameter near the sheet and the temperature is increased. In fact, expanding upsides of slip parameter makes the less hotness move to the surface and it might be the justification behind diminishing sense in the velocity.

For both the Carreau and Casson fluid cases, Fig. 5(a-b) illustrates the influence of thermal slip (S_T) on the velocity and temperature profiles. The improvement S_T is shown to contribute to temperature drop, but the coefficient of thermal accommodation increases. Because of temperature changes, this will decrease the thermal diffusion in the flow area and even get thinner.

The results of Prandtl number (Pr) on the velocity and temperature profiles for both the Carreau and Casson fluid cases are shown in Fig. 6(a-b). The graphs demonstrate that as the Pr values rise, the temperature and speed decrease. The ratio of momentum diffusivity to thermal diffusivity is signified by the Prandtl number. Because of the fact that the higher Prandtl liquid has poor thermal conductivity, which lowers conduction and hence the thickness of the thermal boundary layer and reduces temperature as a result.

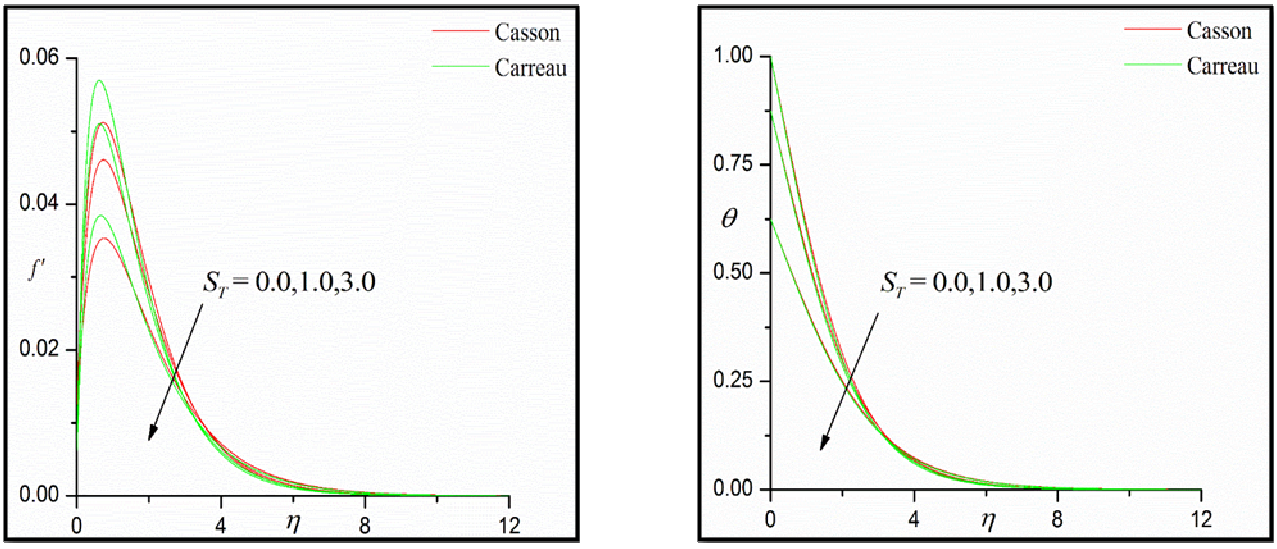

(a) (b)

Fig. 5. Effects of thermal slip parameter on the (a) velocity (b) temperature

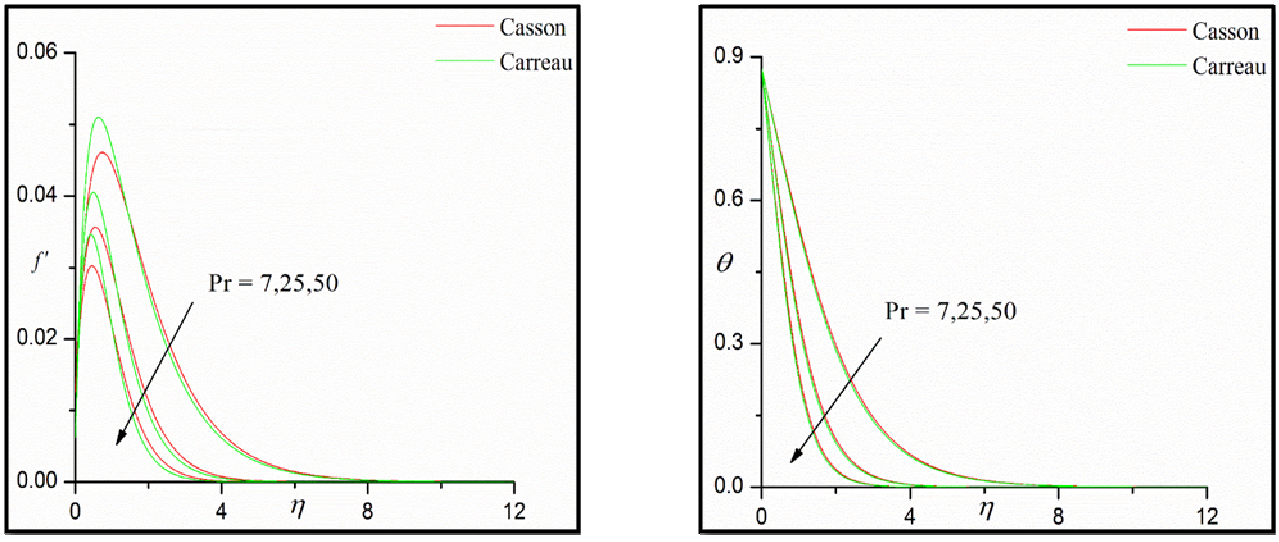

(a) (b)

Fig. 6. Effects of Prandtl number on the (a) velocity (b) temperature

The Carreau and Casson fluid situations, the variance in velocity and temperature fields due to the effect of Da are seen in Fig. 7(a-b). With the increase of the Darcy number as seen in Fig. 7(a), the velocity is obviously dramatically decreased greater permeability of the regime leads to a decrease in Darcian drag strength. With the increasing of Da, the velocity peaks near the cylinder surface are often observed to be dis-placed further from the wall. As seen in Fig. 7(b), the temperature rises very significantly with an increase in Da. The gradual decrease in solid fibers with high Da values in the porous medium serves to decrease the heat transfer of thermal conduction in the system.

For different estimations of the Forchheimer inertial drag parameter (Λ) with spiral arrangement η, Fig. 8(a) describes the velocity field (f') response. In the dimensionless energy conservation condition (9), the Forchheimer drag drive concept is quadratic and with an expansion in Λ (which is literally associated with the geometry of the permeable medium) and it would increase. Fig. 8(b) reveals that temperature (θ) persistently spreads from the cylindrical surface with an expansion in Λ across the boundary layer. Through way of heat conduction and convection, the heat would be diffused more viably with stream deceleration. Subsequently, with expanding Λ, the boundary layer administration will be warm and the thickness of the border stratum will be increased, contrasted and the thickness of the velocity boundary layer being diminished.

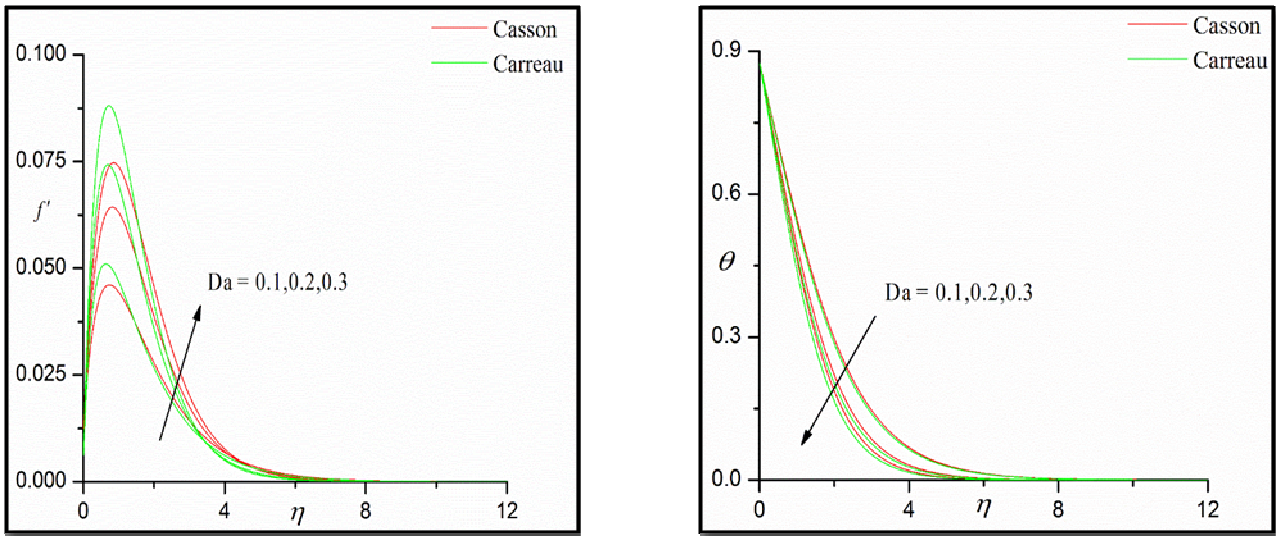

(a) (b)

Fig. 7. Effects of Darcy number on the (a) velocity (b) temperature

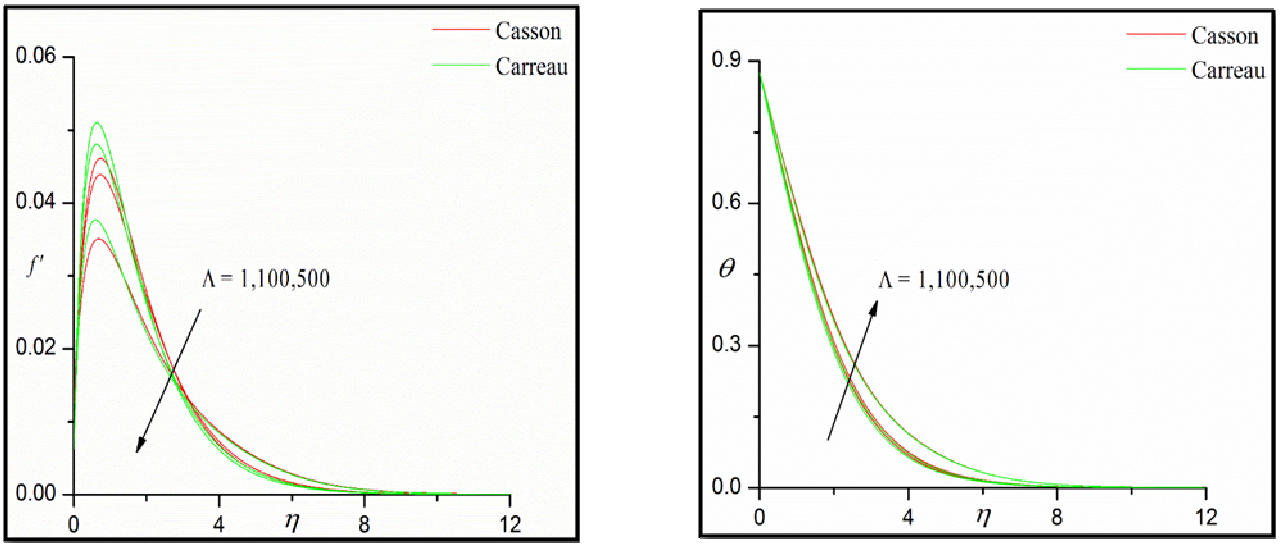

(a) (b)

Fig. 8. Effects of Forchheimer parameter on the (a) velocity (b) temperature

The effect of the stream wise (tangential) coordinates ξ, on the distributions of velocity and temperature is seen in Fig. 9(a-b). A poor deceleration in the flow of the boundary layer is experienced with better ξ, i.e. principles among a progressive space from the lower stagnation point $(\xi = 0)$ along the cylinder surface, as seen in Fig. 9a. Therefore, with ξ values, momentum boundary layer thickness is elevated slightly. Conversely, in Fig. 9b, with increasing ξ values, a weak rise in temperature is measured. Therefore, the thickness of the thermal boundary layer is improved as we advance upward from the minor stagnation point on the plane of the cylinder along the periphery of the cylinder.

The magnetic parameter (M) effect on the shear stress and the rate of heat transfer is shown in Fig. 10 (a-b). Important loss is caused by a higher magnetic field in skin friction (Fig.10a), leading to a delay in boundary layer movement. Therefore, maximal skin friction is obtained only in the deficiency of a radial magnetic field, i.e. $M = 0$. For $M < 1$, the viscous hydrodynamic force in the regimen is surpassed by the magnetic body force. For $M > 1$, the reverse is the case. The decrease in the heat transfer rate with higher M values means that the heat transfer from the boundary layer to the wall (cylinder surface) is decreased. Physically means that more heat is transferred to the fluid from the cylinder surface, which describes the higher temperatures in the earlier computations consistent with intense magnetic fields (Fig. 4b). Thus, in electrically conducting polymer dynamics, the magnetic field is a powerful mechanism for controlling thermal and velocity characteristics.

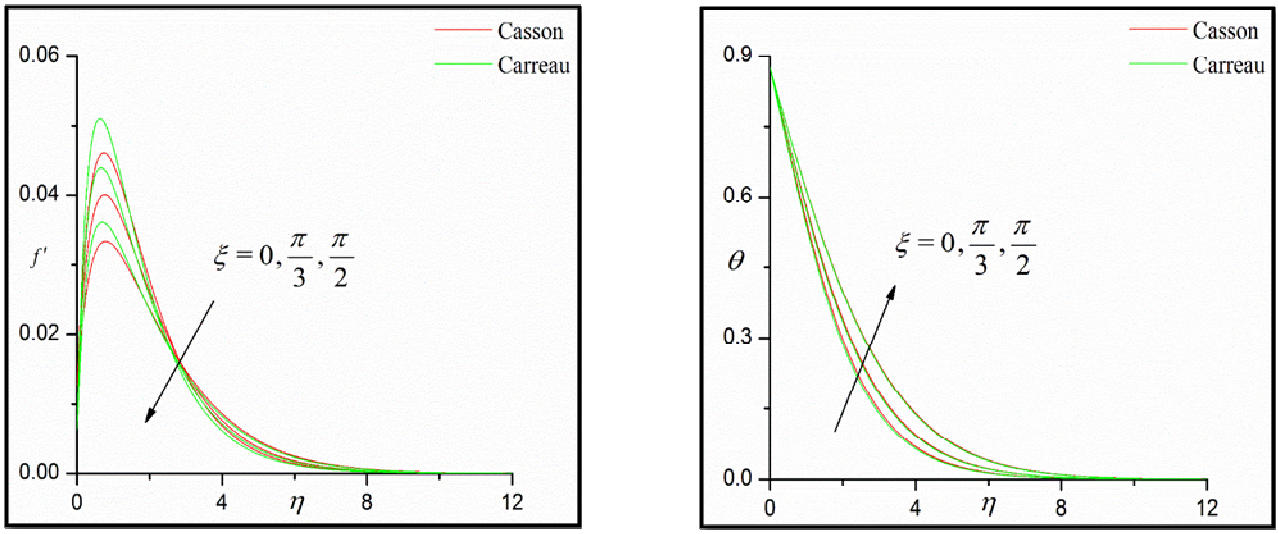

(a) (b)

Fig. 9. Effects of ξ on the (a) velocity (b) temperature

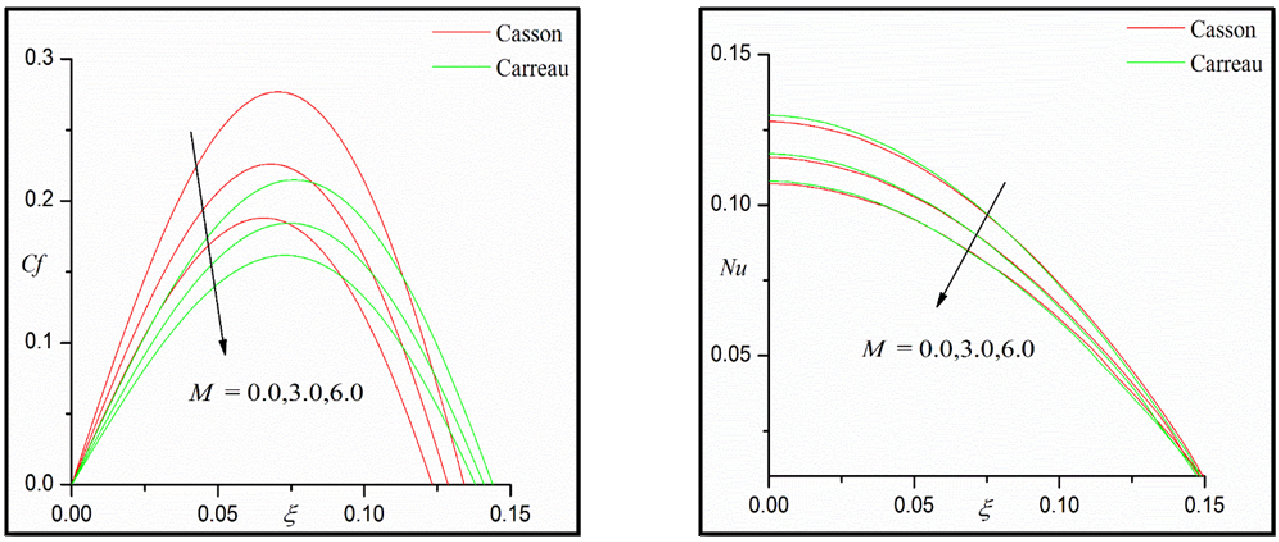

(a) (b)

Fig. 10. Effects of MHD parameter on the (a) skin friction (b) Nusselt Number

The results of velocity slip on skin friction coefficient and number distributions of Nusselt are described in Fig. 11(a-b). It is noted from these graphs that the increasing velocity slip parameter decreases the wall velocity, but for the wall temperature, the opposite pattern is observed. Physically, it can be perceived that the resistance between the liquid and sheet is decreased for higher slip parameter values, and liquid behaves like inviscid liquid leading to full slip.

Fig. 12a-b provides the effect of thermal slip on skin friction coefficient and Nusselt number profile. From Fig. 12a, it is clearly observed that the wall velocity decreases as an increase in the thermal slip parameter. You will see the same results in Fig. 12b for the Nusselt number. On the wall, the greatest impact is detected.

Fig. 13(a-b) demonstrates the effect of Darcian porosity (Da) on the distribution of the skin friction coefficient and heat transfer volume. If the parameter of Darcian porosity is $Da \to \infty$, the Darcian drag force disappears in the momentum equation (15) in that case. In relation to Da (which reflects dimensionless permeability, i.e. hydraulic conductivity), however, the porosity parameter exists in Eq. (15) in a variety of terms. As expected, increasing Da (Fig. 13a) reduces the amount of solids present to withstand the flow and accelerates the coefficient of skin friction and heat transfer rate as well (Fig. 13b). Thermal boundary layers are thus decreased with higher porosity in thickness and are thickened for materials that engulf low-porosity.

The skin friction coefficient and Nusselt number profiles are analyzed from Figs. 14(a-b) for the Forchheimer parameter inciting value. It can be shown that with an increasing value of the Forchheimer parameter, both the velocity and temperature at the wall are reduced.

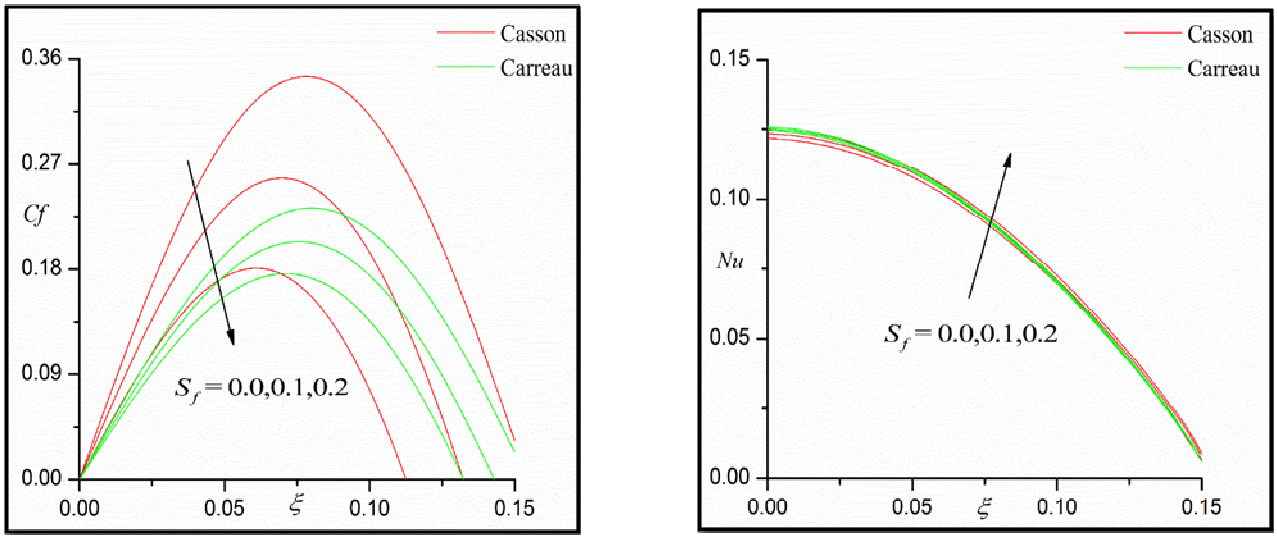

Fig. 11. Effects of velocity slip parameter on the (a) skin friction (b) Nusselt Number

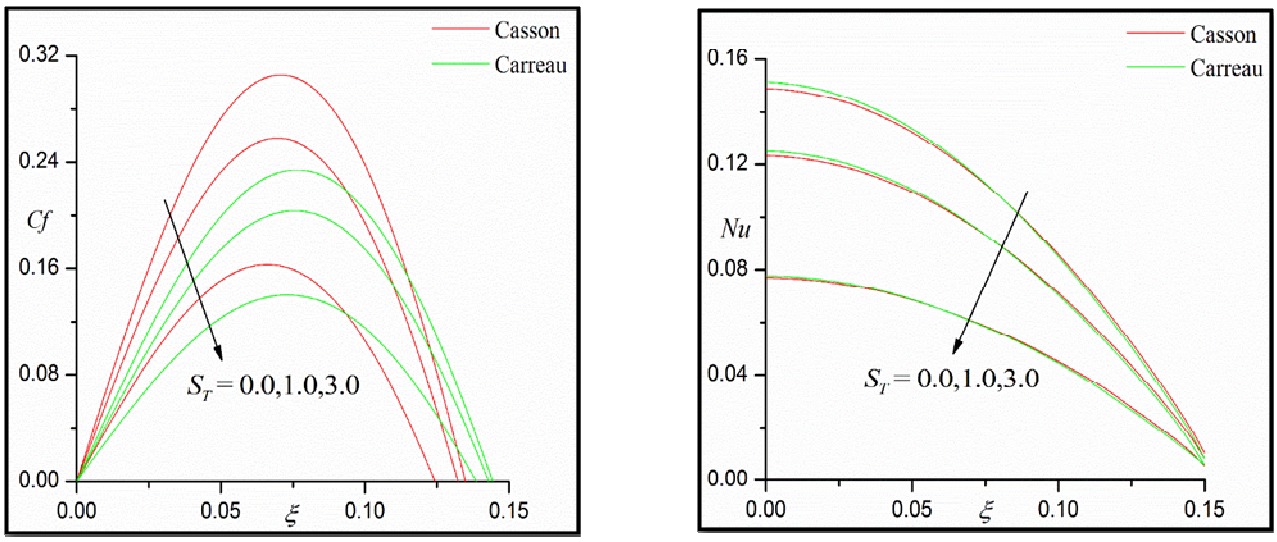

Fig. 12. Effects of thermal slip parameter on the (a) skin friction (b) Nusselt Number

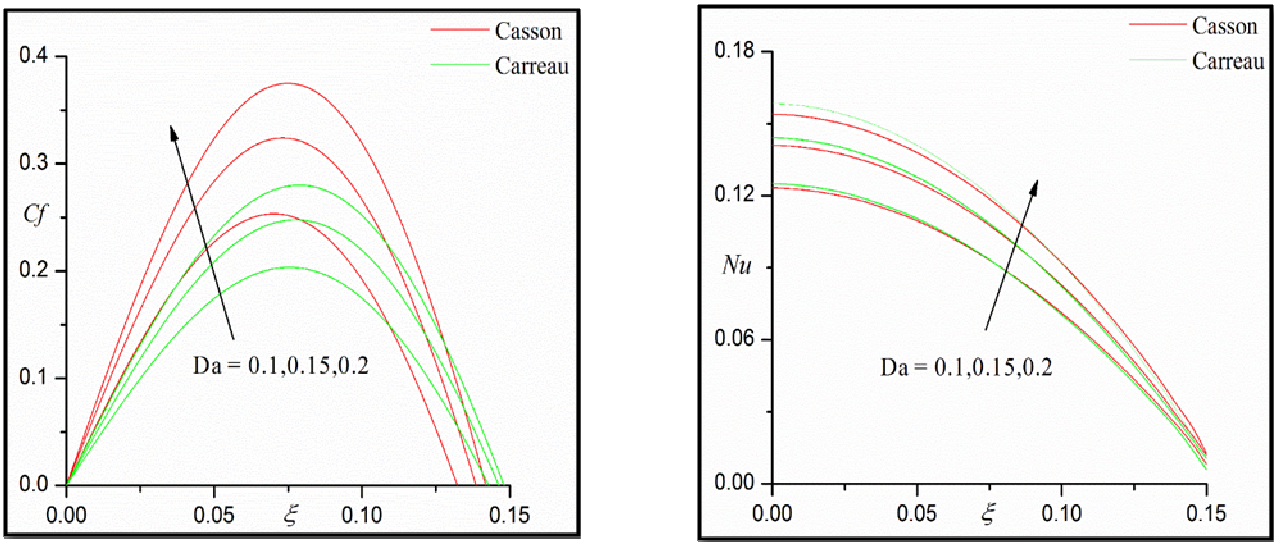

(a) (b)

Fig. 13. Effects of Darcy number on the (a) skin friction (b) Nusselt Number

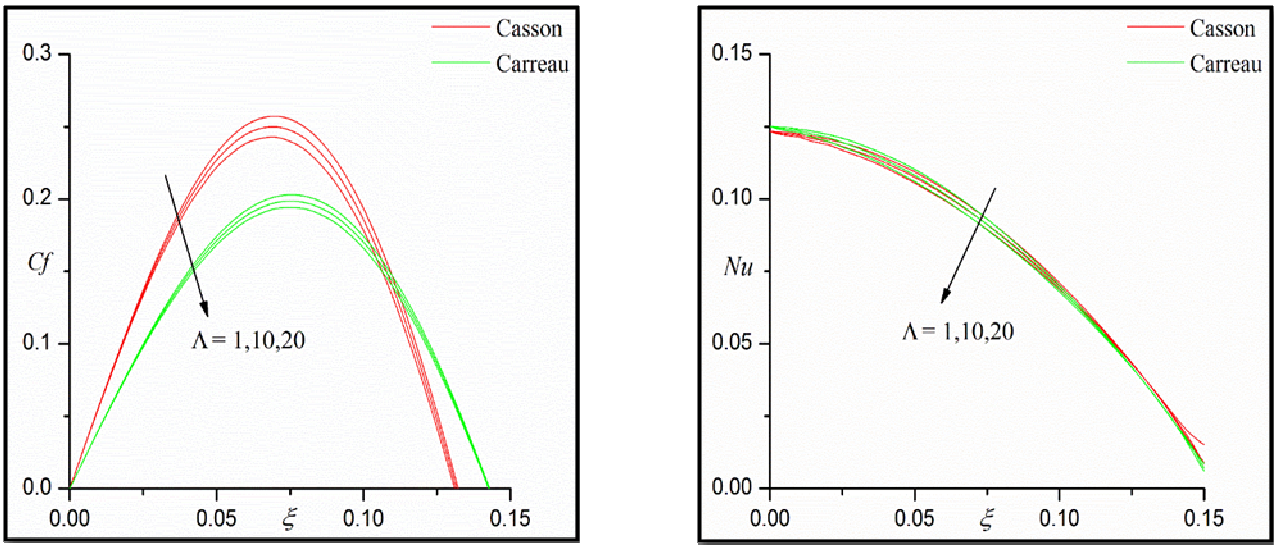

(a) (b)

Fig. 14. Effects of Forchheimer parameter on the (a) skin friction (b) Nusselt Number

Table 2. Values of C_f and Nu for different Pr and β

Pr	$\beta = 1.0$		$\beta = 3.0$		$\beta = 5.0$	
	C_f	Nu	C_f	Nu	C_f	Nu
7	0.2048	0.3076	0.1893	0.3098	0.1839	0.3109
10	0.1978	0.3597	0.1844	0.3624	0.1795	0.3638
15	0.1889	0.4266	0.1781	0.4326	0.1737	0.4344
25	0.1763	0.5295	0.1691	0.5342	0.1654	0.5402
50	0.1573	0.7072	0.1553	0.7103	0.1528	0.7133
75	0.1448	0.8360	0.1442	0.8372	0.1440	0.8388
100	0.1355	0.9397	0.1344	0.9401	0.1281	0.9491

Table 3. Values of C_f and Nu for different Pr and We

Pr	$We = 0.0$		$We = 1.0$		$We = 3.0$	
	C_f	Nu	C_f	Nu	C_f	Nu
7	0.1740	0.3129	0.1337	0.3127	0.0499	0.3128
10	0.1702	0.3659	0.1317	0.3661	0.0440	0.3662
15	0.1653	0.4360	0.1290	0.4364	0.0392	0.4371
25	0.1582	0.5416	0.1250	0.5421	0.0353	0.5427
50	0.1472	0.7139	0.1183	0.7212	0.0325	0.7209
75	0.1399	0.8463	0.1138	0.8485	0.0309	0.8486
100	0.1343	0.9473	0.1102	0.9491	0.0289	0.9500

Table 4. Values of C_f and Nu for different Λ

Λ	Newtonian fluid		Casson fluid		Carreau fluid	
	C_f	Nu	C_f	Nu	C_f	Nu
0	0.1740	0.3130	0.2048	0.3076	0.1621	0.3126
1	0.1738	0.3125	0.2045	0.3073	0.1618	0.3122
5	0.1728	0.3103	0.2031	0.3051	0.1610	0.3104
10	0.1715	0.3082	0.2014	0.3051	0.1599	0.3082
50	0.1632	0.2931	0.1895	0.3034	0.1527	0.2932
100	0.1555	0.2795	0.1778	0.2905	0.1459	0.2797
300	0.1376	0.2527	0.1481	0.2503	0.1301	0.2530
500	0.1283	0.2376	0.1308	0.2354	0.1218	0.2376

5. Conclusion

This finding agrees with the slip effect by porous medium on the MHD Casson-Carreau liquid stream past a circular cylinder. We have found the numerous slip effects to make the action of the flow more entertaining. Along with wall skin friction and local Nusselt numbers, the effects of various dimensionless parameters on momentum and thermal fields are explored with the aid of charts and tables. The findings of the present review are as follows:

- In Casson fluid, the rate of heat transfer is higher relative to the case of Carreau fluid. We may infer from this, the Casson fluid is very useful for higher heat transfer appliances. The wall thickness parameter depreciates temperature field for Casson and Carreau fluid cases.
- The increasing values of the velocity slip parameter boost the temperature fields, while the velocity profiles are depreciated.
- Compared with the case of Casson fluid, the thermal boundary layer is strong in Carreau fluid. This proves that in supporting temperature fields, the Carreau fluid is very helpful.

Time-dependent and mass transfer (species diffusion) effects, which are also significant in polymer production, have been ignored in the current study and will be studied in the future.

Author Contributions

N. Nagendra identified and planned the mathematical modeling; B. Venkateswarlu examined the theory of validation; Z. Boulahia supervised the physical interpretation of the results; Ch. Amanulla & G.K Ramesh carried out the solution and graphical procedure. The manuscript was written through the contribution of all authors. All authors discussed the results, reviewed and approved the final version of the manuscript.

Acknowledgments

Not applicable.

Conflict of Interest

The authors declared no potential conflicts of interest concerning the research, authorship, and publication of this article.

Funding

The authors received no financial support for the research, authorship, and publication of this article.

Data Availability Statements

The datasets generated and/or analyzed during the current study are available from the corresponding author on reasonable request.

Nomenclature

B_0	Externally imposed radial magnetic field Skin		***Greek Symbols***
C_f	friction coefficient	α	Thermal diffusivity
f	Non-dimensional stream function	β	Thermal expansion coefficient

Gr	Grashof number
g	Acceleration due to gravity
k	Thermal conductivity of fluid
K_0	Thermal jump factor
Nu	Local Nusselt number
M	Magnetic body force parameter
Pr	Prandtl number
N_0	Velocity (momentum) slip factor
S_f	Velocity slip parameter
S_T	Thermal jump parameter
T	Temperature
u,v	Velocity components along x,y directions
We	Weissenberg (viscoelasticity) number'
x	Stream wise coordinate
y	Transverse coordinate
η	Dimensionless transverse coordinate
ν	Kinematic viscosity
θ	Non-dimensional temperature
ρ	Density viscoelastic fluid
σ	Electrical conductivity of viscoelastic fluid
ξ	Dimensionless steam wise coordinate
ψ	Dimensionless stream function

Subscripts

Γ	Time-dependent material constant
w	Conditions on the wall
∞	Free steam conditions

References

[1] Livescu, S., Mathematical Modeling of Thixotropic Drilling Mud and Crude Oil Flow in Wells and Pipelines–A review, *Journal of Petroleum Science and Engineering*, 98/99, 2012, 174–184.

[2] Hron, J., Málek, J., Pustějovská, P., Rajagopal, K.R., On the Modelling of the Synovial Fluid, *Advances in Tribology*, 2010, Article ID 104957.

[3] Loix, F., Orgéas, L., Geindreau, C., Badel, P., Boisse, P., Bloch, J.F., Flow of Non-Newtonian Liquid Polymers Through Deformed Composites Reinforcements, *Composites Science and Technology*, 69, 2009, 612–619.

[4] Kechichian, V., Crivellari, G.P., Gut, J.A.W., Tadini, C.C., Modelling of Continuous Thermal Processing of a Non-Newtonian Liquid Food under Diffusive Laminar Flow in a Tubular System, *International Journal of Heat and Mass Transfer*, 55, 2012, 5783–5792.

[5] Mukhopadhyay, S., Casson Fluid Flow and Heat Transfer over a Non-Linearly Stretching Surface, *Chinese Physics B*, 22(7), 2013, 1–5.

[6] Eldabe, N.T., Saddeck, G., Elsayed, A.F., Heat Transfer of MHD Non-Newtonian Casson Fluid Flow between Two Rotating Cylinders, *Mechanics and Mechanical Engineering,* 64, 1995, 41–64.

[7]Pramanik, S., Casson Fluid Flow and Heat Transfer Past an Exponentially Porous Stretching Surface in Presence of Thermal Radiation, *Ain Shams Engineering Journal,* 5, 2014, 205–212.

[8] Ghannam, G., Esmail, N., Flow Behavior of Enhanced Oil Recovery Alcoflood Polymers, *Journal of Applied Polymer Science*, 85 (14), 2002, 2896–2904.

[9] Tassaddiq, A., Khan, I., Nisar, K.S., Singh, J., MHD Flow of a generalized Casson Fluid with Newtonian Heating: A Fractional Model with MIttag-Leffler Memory, *Alexandria Engineering Journal*, 59(5), 2020, 3049–3059.

[10] Ramzan, M., Shaheen, N., Chung, J.D., Kadry, S., Chu, Y.M., Howari, F., Impact of Newtonian Heating and Fourier and Fick's Laws on a Magnetohydrodynamic Dusty Casson Nanofluid Flow with Variable Heat Source/Sink over a Stretching Cylinder, *Scientific Reports*, 11, 2021, 2357.

[11] Nazeer, M., Ahmad, F., Ali, W., Saleem, M.I., Khaliq, Z., Chu, Y.M., Perturbation and Numerical Solutions of Non-Newtonian Fluid Bounded with in a Porous Channel: Applications of Pseudo-Spectral Collocation Method, *Numerical Methods for Partial Differential Equations,* 2020, 1-15.

[12] Nazeer, M., Khan, M.I., Kadry, S., Chu, Y.M, Ahmad, F., Ali, W., Irfan, M., Shaheen, M., Regula Perturbation Solution of Couette Flow (Non-Newtonian) between Two Porous Plates: A Numerical Analysis with Irreversibility, *Applied Mathematics and Mechanics (English Edition)*, 42, 2021, 127–142.

[13] Ansari, MD. S., Otegbeye, O., Trivedi, M., Goqo, S.P., Magnetohydrodynamic Bio-Convective Casson Nanofluid Flow: A Numerical Simulation by Paired Quasilinearization, *Journal of Applied and Computational Mechanics*, 5(4), 2021, 2024-2039.

[14] Trivedi, M., Otegbeye, O., Ansari, MD.S., Motsa, S.S., A Paired Quasilinearization on Magnetohydrodynamic Flow and Heat Transfer of Casson Nanofluid with Hall Effects, *Journal of Applied and Computational Mechanics,* 5(5), 2019, 849-860.

[15] Venkateswarlu, B., Satya Narayana, P.V., Cu-Al2O3/H2O Hybrid Nanofluid Flow past a Porous Stretching Sheet due to Temperature Dependent Viscosity and Viscous Dissipation, *Heat Transfer*, 50(1), 2021, 432-449.

[16] Venkateswarlu, B., Satya Narayana, P.V., Variable Wall Concentration and Slip Effects on MHD Nanofluid Flow Past a Porous Vertical Plate, *Journal of Nanofluids*, 8(4), 2019, 838-844.

[17] Casson, N., *A Flow Equation for Pigment Oil-Suspensions of the Printing Ink Type,* In: Mill, C.C., Ed., Rheology of Disperse Systems (C.C. Mill, ed.), Pergamon Press, London, 1959, 84–104.

[18] Bird, R.R., Dai, G.C., Yarusso, B.J., The Rheology and Flow of Viscoplastic Materials, *Review in Chemical Engineering*, 1, 1983, 1–83.

[19] Hayat, T., Pop., I., Hendi, A.A., Stagnation-point Flow and Heat Transfer of a Casson Fluid Towards a Stretching Sheet, *Zeitschrift fur Naturforschung A,* 67, 2012, 70–76.

[20] Nasir, M.S., Butt, A.S., Ali, A., Unsteady Chemically-Reacting Casson Fluid Flow in an Irregular Channel with Convective Boundary, *Zeitschrift fur Naturforschung A*, 70(8), 2015, 10–18.

[21] Venkateswarlu, B., Satya Narayana, P.V., Influence of Variable Thermal Conductivity on MHD Casson Fluid Flow over a Stretching Sheet with Dissipation, Soret and Dufour Effects, *Frontiers in Heat and Mass Transfer*, 7, 3016, 1-16.

[22] Venkateswarlu, B., Satya Narayana, P.V., Chemical Reaction and Radiation Absorption Effects on the Flow and Heat Transfer of Nanofluid in a Rotating System, *Applied Nanoscience,* 5(3), 2015, 351-360.

[23] Khellaf, K., Lauriat, G., Numerical Study of Heat Transfer in a Non-Newtonian Carreau-Fluid between Rotating Concentric Vertical Cylinders, *Journal of Non-Newtonian Fluid Mechanics*, 89, 2000, 45–61.

[24] Khan, M., Hashim, Hussain, M., Azam, M., Magnetohydrodynamic Flow of Carreau Fluid over a Convectively Heated Surface in the Presence of Non-Linear Radiation, *Journal of Magnetism and Magnetic Materials*, 412, 2016, 63–68.

[25] Raju, C.S.K., Sandeep, N., Falkner-Skan Flow of a Magnetic-Carreau Fluid Past a Wedge in the Presence of Cross Diffusion Effects, *The European Physical Journal Plus,* 131, 2016, 267.

[26] Akbar, N.S., Nadeem, S., Ul Haq, R., Ye, S., MHD Stagnation Point Flow of Carreau Fluid toward a Permeable Shrinking Sheet: Dual Solutions, *Ain Shams Engineering Journal*, 5(4), 2014, 1233–1239.

[27] Abbas, T., Rehman, S., Ali, R.S, Idrees, M., Qayyum, M., Analysis of MHD Carreau Fluid Flow over a Stretching Permeable Sheet with Variable Viscosity and Thermal Conductivity, *Physica A: Statistical Mechanics and its Applications*, 551, 2020, 124225.

[28] Azam, M., Xu, T., Mabood, F., Khan, M., Non-linear Radiative Bioconvection Flow of Cross Nano-material with Gyrotactic Microorganism and Activation Energy, *International Communication in Heat and Mass Transfer*, 127, 2021, 105530

[29] Song, Y.Q., Waqas, H., Al-Khaled, K., Farooq, U., Khan, S.U., Khan, M.I., Chu, Y.M., Qayyum, S., Bioconvection Analysis for Sutter by Nanofluid over an Axially Rigid Cylinder with Melting Heat Transfer and Variable Thermal Features: A Marangoni and Solutal Model, *Alexandria Engineering Journal*, 60, 2021, 4663-4675.

[30] Malik, M.K., Salahuddin, T., Hussain, A., Bilal, S., Awais, M., Homogeneous-Heterogeneous Reactions in Williamson Fluid Model over a Stretching Cylinder by using Keller Box Method, *AIP Advances,* 5, 2015, 107227.

[31] Azam, M., Xu, T., Shakoor, A., Khan, M., Effects of Arrhenius Activation Energy in Development of Covalent Bonding in Axisymmetric Flow of Radiative-Cross Nanofluid, *International Communication in Heat and Mass Transfer*, 113, 2020, 104547.

[32] Azam, M., Mabood, F., Xu, T., Waly, M., Tlili, I., Entropy Optimized Radiative Heat Transportation in Axisymmetric Flow of Williamson Nanofluid with Activation Energy, *Results in Physics*, 19(3), 2020, 103576.

[33] Rehman, K.U. Khan, A.A., Malik, M.Y., Ali, U., Naseer, M., Numerical Analysis Subject to Double Stratification and Chemically Reactive Species on

Williamson Dual Convection Fluid Flow Yield by an Inclined Stretching Cylindrical Surface, *Chinese Journal of Physics*, 55, 2017, 1637-1652.
[34] Alsemiry, R.D., Sayed, H.M., Amin, N., Mathematical Analysis of Carreau Fluid Flow and Heat transfer within an Eccentric Catheterized Artery, *Alexandria Engineering Journal*, 61(1), 2022, 523-539.
[35] Afzal, S., Siddique, I., Jarad, F., Ali, R., Abdal, S., Hussain, S., Significance of Double Diffusion for Unsteady Carreau Micropolar Nanofluid Transportation Across an Extending Sheet with Thermo-Radiation and Uniform Heat Source, *Case Studies in Thermal Engineering*, 28, 2021, 101397
[36] Bilal, M., Saeed, A., Gul, T., Rehman, M., Khan, A., Thin Film Flow of Carreau Fluid over a Stretching Surface Including the Couple Stress and Uniform Magnetic Field, *Partial Differential Equations in Applied Mathematics*, 4, 2021, 100162.
[37] Shehzad, S.A., Madhu, M., Shashi Kumar, N.S., Gireesha, B.J., Mahanthesh, B., Thermal and Entropy Generation of Non-Newtonian Magneto-Carreau Fluid Flow in Microchannel, *Journal of Thermal Analysis and Calorimetry*, 143, 2021, 2717-2727.
[38] Noreen, S., Kausar, T., Tripathi, D., Ul Ain, Q., Lu, D.C., Heat Transfer Analysis on Creeping Flow Carreau Fluid Driven by Peristaltic Pumping in an Inclined Asymmetric Channel, *Thermal Science and Engineering Progress*, 17(1), 2020, 100486.
[39] Raza, J., Thermal Radiation and Slip Effects on Magnetohydrodynamic (MHD) Stagnation Point Flow of Casson Fluid over a Convective Stretching Sheet, *Propulsion and Power Research*, 8(2), 2019, 138–146.
[40] Santoshi, P.N., Ramana Reddy, G.V., Padma, P., Numerical Scrutinization of Three Dimensional Casson-Carreau Nanofluid Flow, *Journal of Applied and Computational Mechanics*, 6(2), 2020, 531-542.
[41] Nagendra, N., Amanulla, CH., Sudhakar Reddy, M., Slip Effects on MHD Flow of a Williamson Fluid from an Isothermal Sphere: A Numerical Study, *Modelling Measurement and Control B,* 86(3), 2017, 782-807.
[42] Amanulla, CH., Wakif, A., Saleem, S., Numerical Study of a Williamson Fluid Past a Semi-Infinite Vertical Plate with Convective Heating and Radiation Effects, *Diffusion Foundations*, 28, 2020, 1-15.
[43] Liu, Y., Gehde, M., Effects of Surface Roughness and Processing Parameters on Heat Transfer Coefficient between Polymer and Cavity Wall During Injection Molding, *International Journal of Advanced Manufacturing Technology*, 84, 2016, 1325–1333.
[44] Hatzikiriakos, S.G., Mitsoulis, E., Slip Effects in Tapered Dies, *Polymer Engineering and Science*, 49(10), 2009, 1960–1969.
[45] Sparrow, E.M., Lin, S.H., Laminar Heat Transfer in Tubes under Slip-Flow Conditions, *ASME Journal of Heat Transfer,* 84, 1962, 363–639.
[46] Subba Rao, A., Prasad, V.R., Bhaskar Reddy, N., Bég, O.A., Heat Transfer in a Casson Rheological Fluid from a Semi-Infinite Vertical Plate with Partial Slip, *Heat Transfer Asian Research*, 44(3), 2015, 272–291.
[47] Uddin, MD.J., Khan, W.A., Ismail, A.I.MD., Bég, O.A., Computational Study of Three-Dimensional Stagnation Point Nanofluid Bio-Convection Flow on a Moving Surface with Anisotropic Slip and Thermal Jump Effects, *ASME Journal of Heat Transfer,* 138(10), 2016, 104502.
[48] Madhu, M., Mahanthesh, B., Shashi Kumar, N.S., Shehzad, S.A., Khan, S.U., Gireesha, B.J., Performance of Second Law in Carreau Fluid Flow by an Inclined Microchannel with Radiative Heated Convective Condition, *International Communications in Heat and Mass Transfer*, 117, 2020, 104761.
[49] Salahuddin, T., Carreau Fluid Model towards a Stretching Cylinder: Using Keller Box and Shooting Method, *Ain Shams Engineering Journal,* 11(2), 2020, 495–500.
[50] Mahanthesh, B., Animasaun, I.L., Gorji, M.R., Alarifi, I.M., Quadratic Convective Transport of Dust Casson and Dusty Carreau Fluids Past a Stretched Surface with Nonlinear Thermal Radiation, Convective Condition and Non-Uniform Heat Source/Sink, *Physica A: Statistical Mechanics and its Applications*, 535(1), 2019, 122471.
[51] Amanulla, CH., Wakif, A., Boulahia, Z., Reddy, M.S., Nagendra, N., Numerical Investigations on Magnetic Field Modeling for Carreau Non-Newtonian Fluid Flow Past an Isothermal Sphere, *Journal of the Brazilian Society of Mechanical Sciences and Engineering*, 40, 2018, 462.
[52] Gireesha, B.J., Kumar, P.B.S., Mahanthesh, M., Shehzad, S.A., Rauf, A., Nonlinear 3D Flow of Casson-Carreau Fluids with Homogeneous-Heterogeneous Reactions: A Comparative Study, *Results in Physics*, 7, 2017, 2762–2770.
[53] Khan, M., Irfan, M., Khan, W.A., Alshomrani, A.S., A New Modeling for 3D Carreau Fluid Flow Considering Nonlinear Thermal Radiation, *Results in Physics*, 7, 2017, 2692–2704.
[54] Rao, A.S., Nagendra, N., Amanulla, C.H., Surya Narayana Reddy, M., Beg, O.A., Computational Analysis of Non-Newtonian Boundary Layer Flow of Nanofluid Past a Vertical Plate with Partial Slip, Modelling, *Measurement and Control B*, 86(1), 2017, 271-295.
[55] Beg, O.A., Rao, A.S., Amanulla, C.H., Nagendra, N., Suryanarayana Reddy, M., Kadir, A., Numerical Study of Hydromagnetic Non-Newtonian Nanofluid Transport Phenomena from a Horizontal Cylinder with Thermal Slip: Aerospace Nanomaterial Enrobing Simulation, *Journal of Nanofluids*, 7(1), 2018, 115–128.
[56] Cebeci, T., Bradshaw, P., *Physical and Computational Aspects of Convective Heat Transfer*, Springer, New York, 1984.
[57] Keller, H.B., *A New Difference Method for Parabolic Problems,* In: Bramble J (Ed) Numerical Methods for Partial Differential Equations, Academic Press, New York, 1970.
[58] Merkin, Free Convection Boundary Layer on an Isothermal Horizontal Circular Cylinders, ASME/AIChE, *Heat Transfer Conference*, St. Louis, Mo., U.S.A., 1976, 9–11.
[59] Molla, M.M., Saha, S.C., Khan, M.A.I., Hossain, M.A., Radiation Effects on Natural Convection Laminar Flow From a Horizontal Circular Cylinder, *Desalination and Water Treatment,* 30(1-3), 2011, 89–97.
[60] Javed, T., Majeed, A., Mustafa, I., MHD Effects on Natural Convection Laminar Flow from a Horizontal Circular Cylinder in Presence of Radiation, *Revista Mexicana de Fisica*, 61, 2015, 450–457.

ORCID iD

N. Nagendra https://orcid.org/0000-0002-5412-694X
B. Venkateswarlu https://orcid.org/0000-0001-8843-5938
Z. Boulahia https://orcid.org/0000-0001-9528-4955
CH. Amanulla https://orcid.org/0000-0002-8755-1459
G.K. Ramesh https://orcid.org/0000-0001-9404-2823

How to cite this article: Nagendra, N., Venkateswarlu, B., Boulahia, Z., Amanulla, CH., Ramesh, G.K. Magneto Casson-Carreau Fluid Flow through a Circular Porous Cylinder with Partial Slip, *J. Appl. Comput. Mech.*, 8(4), 2022, 1208–1221. https://doi.org/10.22055/JACM.2021.38390.3215